THE JOURNAL OF PHYSICAL CHEMISTRY C

Article

pubs.acs.org/JPCC

Understanding the Conduction Mechanism of the Protonic Conductor CsH_2PO_4 by Solid-State NMR Spectroscopy

Gunwoo Kim,[†,‡] Frédéric Blanc,[†,‡] Yan-Yan Hu,[†,‡] and Clare P. Grey*[,†,‡]

[†]Department of Chemistry, University of Cambridge, Lensfield Road, Cambridge CB2 1EW, United Kingdom

[‡]Department of Chemistry, Stony Brook University, Stony Brook, New York 11790-3400, United States

Supporting Information

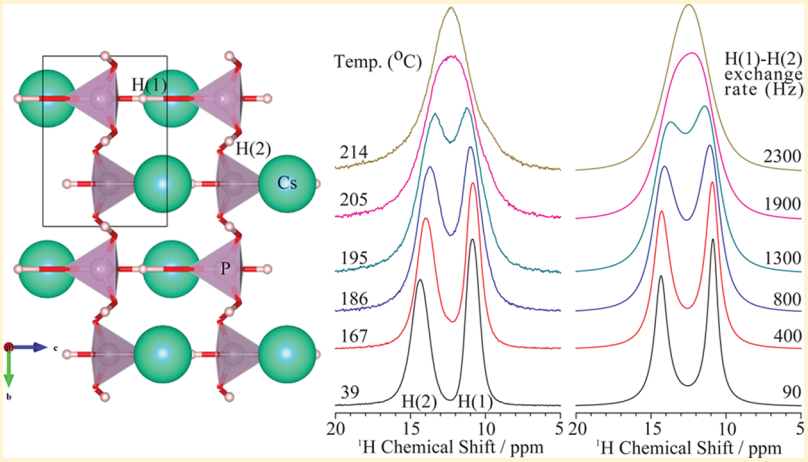

ABSTRACT: Local dynamics and hydrogen bonding in CsH_2PO_4 have been investigated by ^1H, ^2H, and ^{31}P solid-state NMR spectroscopy to help provide a detailed understanding of proton conduction in the paraelectric phase. Two distinct environments are observed by ^1H and ^2H NMR, and their chemical shifts (^1H) and quadrupolar coupling constants (^2H) are consistent with one strong and one slightly weaker H-bonding environment. Two different protonic motions are detected by variable-temperature ^1H MAS NMR and T_1 spin−lattice relaxation time measurements in the paraelectric phase, which we assign to librational and long-range translational motions. An activation energy of 0.70 ± 0.07 eV is extracted for the latter motion; that of the librational motion is much lower. ^{31}P NMR line shapes are measured under MAS and static conditions, and spin−lattice relaxation time measurements have been performed as a function of temperature. Although the ^{31}P line shape is sensitive to the protonic motion, the reorientation of the phosphate ions does not lead to a significant change in the ^{31}P CSA tensor. Rapid protonic motion and rotation of the phosphate ions is seen in the superprotonic phase, as probed by the T_1 measurements along with considerable line narrowing of both the ^1H and the ^{31}P NMR signals.

1. INTRODUCTION

The strong demand for clean energy sources to solve environmental issues has driven a worldwide effort to improve both the conversion and the storage of energy. Fuel cells are promising alternatives to conventional internal combustion engines as they are more efficient and much cleaner. Most systems that have been commercialized so far are based on a proton exchange membrane-type electrolyte but critical limitations remain such as their design complexity, the high cost of the membrane, the use of a Pt catalyst due to the low operating temperatures, and fuel permeation over 100 °C.[1] An alternative strategy is to operate fuel cells in the so-called intermediate temperature range (200−600 °C), which opens up the possibility of finding new, cheaper membranes for use in commercial applications.[2,3]

Among the various possible proton conducting electrolytes,[2] solid inorganic acids of the general formula MH_xXO_4 (M = K, Rb, Tl, Cs, x = 1−2, X = S, P, As, Se) have attracted significant interest as they can operate in fuel cells under relatively dry conditions at moderate temperature ranges (150−300 °C). To date, CsH_2PO_4 is the most promising material,[4−9] and Haile et al.[5] successfully demonstrated on a laboratory scale that it can be used as a solid electrolyte in a direct methanol fuel cell.

CsH_2PO_4 exists in three different crystallographic phases. At low temperatures, CsH_2PO_4 crystallizes in a monoclinic structure in space group $P2_1$ (the so-called ferroelectric phase), transforming into a paraelectric phase (monoclinic, space group $P2_1/m$) above the Curie temperature (−120 °C). In the paraelectric phase, one set of hydrogen bonds, O(1)−H(1)···O(2), connects the tetrahedral PO_4 groups along the a

Received: December 17, 2012
Revised: February 28, 2013
Published: February 28, 2013

   dx.doi.org/10.1021/jp312410t | J. Phys. Chem. C 2013, 117, 6504−6515

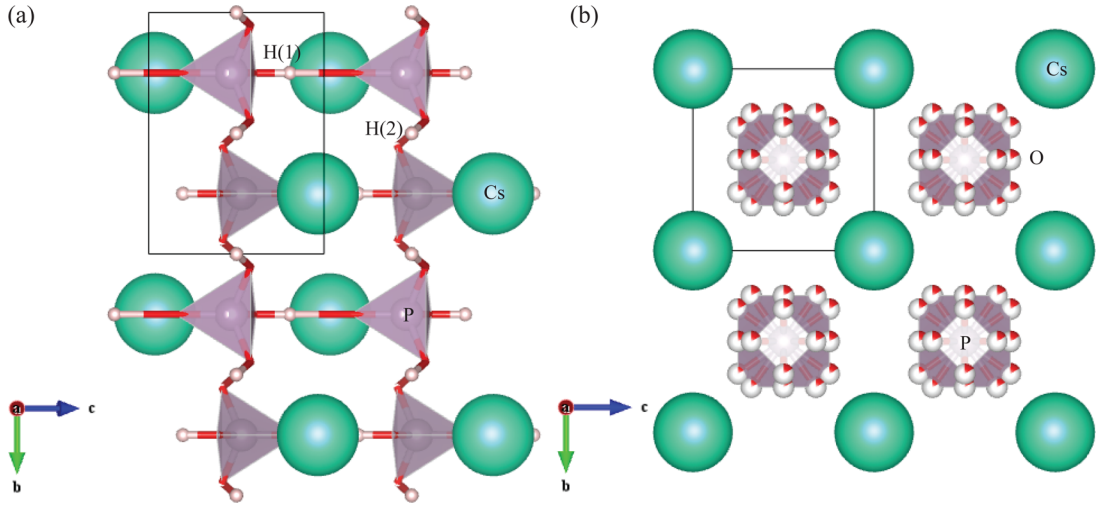

Figure 1. Crystal structures of CsH_2PO_4 in (a) the monoclinic paraelectric phase with space group $P2_1/m$,[10] and (b) the cubic superprotonic phase with space group $Pm\bar{3}m$.[13] The atoms and hydrogen bonds are labeled. In the superprotonic phase, six possible orientations of the phosphate unit are found due to the dynamic disorder, creating partially occupied oxygen positions.

axis, while the second set of hydrogen bonds, O(3)–H(2)···O(3), creates zigzag chains along the *b* axis.[10] At the so-called superprotonic phase transition (230 ± 2 °C),[5,11,12] CsH_2PO_4 transforms into a cubic structure with space group $Pm\bar{3}m$.[10,12−14] Rietveld refinement shows that a CsCl-like cubic structure (a = 4.9549(4) Å) is present with cesium atoms located at the every corner of the cubic unit cell and phosphate ions in the center of the unit cell (Figure 1).[13] An increase of protonic conductivity by up to 4 orders of magnitude (to 0.01 S cm^{-1}) has been observed at this superprotonic phase transition,[12] making this material extremely interesting as a fuel cell electrolyte. Dynamically disordered hydrogen bonds and strongly disordered phosphate anions with multiple, partially occupied oxygen sites, are believed to be responsible for the high protonic conductivity of this phase.[12]

Although questions remain about the nature of the conduction mechanism in these phases, the rapid reorientation of the tetrahedral phosphate ion in the superprotonic phase is believed to facilitate proton conduction.[12] From a macroscopic point of view, AC impedance spectroscopy has clearly shown very different transport properties in the paraelectric and superprotonic phases, but this method cannot establish a relationship between long-range protonic and short-range phosphate motion.[12,15,16] Spectroscopic studies using a large range of techniques, such as quasi-elastic neutron scattering (QENS),[17] nuclear magnetic resonance (NMR),[13,18] and electrochemical impedance spectroscopy,[12,15,17] have been carried out to obtain a better understanding of the proton conduction mechanism in CsH_2PO_4. Two different diffusion coefficients corresponding to librational (2.5×10^{-6} cm^2 s^{-1} at 240 °C) and translational (2.9×10^{-7} cm^2 s^{-1} at 238 °C) diffusion of protons have been observed by QENS and pulsed field gradient (PFG) NMR above the phase transition.[17] A proton jump distance of 2.7 Å was determined, which coincides with the average oxygen jump distance of a reorientating phosphate ion, strongly implying that the protonic motion above the phase transition is correlated with the rotational motion of the phosphate ions. More recently, Car–Parrinello ab initio molecular dynamics studies have shown that the proton hopping rate is faster than the PO_4 ion reorientation.[19] This is in sharp contrast with the mechanism suggested for the related $CsHSO_4$ phase where experimental[20−22] and computational[23−26] approaches demonstrated that the proton hopping between two neighboring SO_4 groups is the rate-limiting step.

Previous results using ^1H and ^{31}P static solid-state NMR techniques on both single crystal and powder CsH_2PO_4 as a function of temperature showed that the dynamics of the phosphate ions can be observed by NMR in the paraelectric phase of CsH_2PO_4.[13] Simulation of the spectra of phosphate anion reorientation based on a simple two-site jump model yielded a jump frequency of 25 kHz at 207 °C. However, it is unclear whether the neglect of the effect of the $^{31}P-^1H$ dipolar coupling (~3 kHz) on the line shape as a function of temperature in this work affects the results. More recently, the ^{31}P centerband-only detection of exchange (CODEX) NMR experiment[18] was used to observe motion in the 10–40 Hz range at 25–50 °C. The geometry of the anionic motion was investigated with this method, but the interpretation of the results was complicated by the interference of the CODEX dephasing by the dipolar coupling to the nearby ^{133}Cs quadrupolar nuclei. Protonic motion was clearly observed in this work by both 2D exchange spectroscopy and double quantum NMR.[18] Because of the hardware limitations, the motion could not be studied at temperatures higher than 50 °C and thus near and at the superprotonic phase transition temperature.

The aim of this Article is to provide a deeper understanding of the hydrogen bonding and dynamic behavior of CsH_2PO_4 as it approaches the paraelectric–superprotonic phase transition, by using variable-temperature multinuclear solid-state NMR spectroscopy, which will ultimately help to understand the proton conduction mechanism in this compound. NMR spectroscopy is ideally suited for such studies as one can observe both the proton charge carrier by ^1H NMR and the phosphate group by ^{31}P NMR because both ^1H and ^{31}P nuclei have a high gyromagnetic ratio, high natural abundance, and are spin 1/2. For example, as shown in other series of solid inorganic acids, ^1H dynamics can be investigated by ^1H line shape analysis and relaxation time measurements as a function of temperature.[22,27−29] In addition, CsH_2PO_4 can be readily deuterated (to form CsD_2PO_4), and ^2H (I = 1) NMR can be performed to probe the hydrogen bonding and deuteron

dx.doi.org/10.1021/jp312410t | J. Phys. Chem. C 2013, 117, 6504−6515

motion.[30−32] Thus, the dynamics over a large time scale (Hz to MHz) can also be accessed by combining various NMR methods (line shape analysis, relaxation times) with variable-temperature measurements,[33,34] to provide further insight into the proton conduction mechanism.

2. EXPERIMENTAL METHODS

2.1. Sample Preparation and Characterization. CsH_2PO_4 was synthesized by using a methanol-induced precipitation method as described previously.[12] CsD_2PO_4 was prepared by dissolution of CsH_2PO_4 (150 mg, 0.652 mmol) in D_2O (4 g, 200 mmol). The solution was then freeze-dried for 7 days, and CsD_2PO_4 was collected. All CsH_2PO_4 samples were stored in a desiccator and dried under vacuum to remove trace amounts of surface water before any measurements. Powder X-ray diffraction measurements were performed on a Scintag diffractometer using Cu Kα radiation (λ = 1.5418 Å), and the room-temperature powder X-ray diffraction patterns of CsH_2PO_4 and CsD_2PO_4 (Figure S1) are consistent with the monoclinic phase (space group $P2_1/m$) reported previously.[10,35] Differential scanning calorimetry (DSC) and thermo gravimetric analysis (TGA) measurements were carried out using a Perkin-Elmer DSC 7 instrument. All measurements were performed under a nitrogen gas flow to minimize contact with air.

2.2. NMR. Ultra fast magic angle spinning (MAS) ^{1}H NMR spectra were obtained at 16.4 T (700 MHz for ^{1}H) on a Bruker Avance III spectrometer equipped with a 1.3 mm HX MAS probehead spinning the sample at a MAS frequency of 60 kHz. A Hahn-echo experiment was carried out using a ^{1}H radio frequency (rf) field amplitude of 83 kHz with a recycle delay of 500 s.

Variable-temperature (VT) ^{1}H and ^{31}P MAS, and ^{2}H static (non spinning) NMR spectra were obtained at 11.7 T on a Varian Chemagnetics Infinity Plus 500 MHz spectrometer using a 4 mm HX Chemagnetics probehead. Variable-temperature ^{31}P NMR spectra were obtained at 8.45 T on a Varian Chemagnetics Infinity Plus 360 MHz spectrometer using a 4 mm HX MAS Chemagnetics probehead under static (non spinning) conditions. Rotor synchronized Hahn-echo experiments were carried out with an evolution period τ set to one rotor period (vide supra). The ^{1}H and ^{31}P rf pulse powers were set to 83 kHz, and ^{31}P spectra were acquired with 80−100 kHz for ^{1}H decoupling. ^{1}H and ^{31}P T_1 longitudinal relaxation times were measured at 4.7 and 11.7 T using the saturation-recovery pulse sequence with a pulse train of 50 pulses separated by 10 ms, which was found adequate to saturate the magnetization. The ^{2}H rf field amplitude was set to 50 kHz, and a quadrupolar echo experiment with a τ interval 20 μs was carried out to record the spectra. A recycle delay of 100 s was used.

All of the samples were packed in ZrO_2 rotors under dry conditions and tightly sealed. Temperature calibration of the probes was performed in a separate MAS experiment using the ^{207}Pb resonance of $Pb(NO_3)_2$.[36,37] The sample temperatures quoted subsequently have all been corrected according to this calibration, and have an accuracy of ±5 °C. Larger errors of more than 10 °C were observed at the high-temperature limit of the temperature control unit (250 °C). Larger errors are also expected for the VT ^{31}P static NMR spectra because the calibration was performed under MAS conditions. ^{1}H and ^{31}P chemical shifts were externally referenced to TMS at 0 ppm and to 85% H_3PO_4 in water at 0 ppm, respectively. NMR data were processed with Matlab and MatNMR.[38] Simulations of ^{1}H two-site exchange process were performed with Mathematica 9. Simulations of the ^{31}P chemical shift anisotropy (CSA) were performed with DMFit,[39] and Spinevolution,[40] and the Haeberlen−Mehring−Spiess convention[41] is used in this work. The isotropic chemical shift δ_{iso}, reduced anisotropy δ_{aniso}, and asymmetry η parameters are defined by:

$$\delta_{iso} = \frac{\delta_{11} + \delta_{22} + \delta_{33}}{3} \quad (1)$$

$$\delta_{aniso} = \delta_{33} - \delta_{iso} \quad (2)$$

$$\eta = \frac{\delta_{22} - \delta_{11}}{\delta_{aniso}} \quad (3)$$

where δ_{11}, δ_{22}, and δ_{33} are the principal components of the shielding tensors (with $\delta_{11} \geq \delta_{22} \geq \delta_{33}$ and $|\delta_{33} - \delta_{iso}| \geq |\delta_{11} - \delta_{iso}| \geq |\delta_{22} - \delta_{iso}|$). Simulations of static ^{2}H line shapes have been performed with Simpson[42] and the NMR WebLab V4.3.2.[43] The quadrupole coupling constant C_Q is defined as

$$C_Q = \frac{eQV_{zz}}{h} \quad (4)$$

where Q is the electric quadrupole moment of the ^{2}H nucleus (2.9×10^{-31} m^2),[44] h is Planck's constant,[34] and the asymmetry parameter η_Q is defined as

$$\eta_Q = \frac{V_{xx} - V_{yy}}{V_{zz}} \quad (5)$$

obtained from the principal components V_{xx}, V_{yy}, V_{zz} ($|V_{zz}| \geq |V_{yy}| \geq |V_{xx}|$) of the electric field gradient tensor.

3. RESULTS

3.1. Assignment of Hydrogen Bonds by ^{1}H and ^{2}H NMR Spectroscopy. The ^{1}H NMR spectrum of CsH_2PO_4 obtained at room temperature and under ultra fast MAS conditions shows two well-resolved resonances with isotropic chemical shifts of 10.9 and 14.3 ppm (1:1 ratio) (Figure 2),

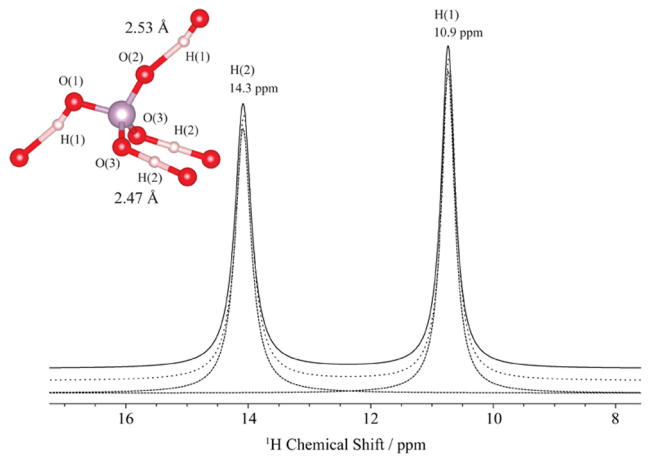

Figure 2. Room-temperature ^{1}H MAS spectrum of CsH_2PO_4 obtained at 16.4 T with a MAS rate of 60 kHz. The experimental spectrum is shown as a full line, while the total fit and spectrum deconvolutions are shown with dashed and dotted lines, respectively. The isotropic chemical shifts and assignments are given above the NMR signals. The inset shows the PO_4 tetrahedron with the O(1)−H(1)···O(2) and O(3)−H(2)···O(3) bond distances (2.53 and 2.47 Å, respectively).[10]

dx.doi.org/10.1021/jp312410t | J. Phys. Chem. C 2013, 117, 6504−6515

corresponding to the two distinct equally populated proton sites in the crystal structure. The peaks are strongly shifted to higher frequency positions consistent with strong hydrogen bonding.[10,35] Similar ^{1}H NMR spectra of CsH_2PO_4 were obtained by Boysen and Haile,[45] although surface-adsorbed water at 6.6 ppm was not observed (Figure S2) under our experimental conditions, indicating that the surface water was quantitatively removed.

The two resonances can be readily assigned by using the known relationship between the isotropic chemical shift and the donor-to-acceptor distance of the hydrogen bond.[46]

$$\delta_{iso}\ (\text{ppm}) = 79.05 - 255d(\text{O}-\text{H}\cdots\text{O})\ (\text{nm}) \quad (6)$$

Table 1 summarizes the previously reported crystallographic data of CsH_2PO_4 obtained by both X-ray and neutron diffraction (ND) methods, in the paraelectric phases.[10,35,47−52] Note that the hydrogen-bond distances measured by XRD and ND are slightly different, which may be due to a H−D isotope effect.[53−55] Making use of the more recent O−H···O distance determined from the XRD data,[10] ^{1}H chemical shifts of 14.5 and 16.1 ppm could be estimated for the H(1) and H(2) protons (Table 1 and eq 6). A larger separation in chemical shifts is seen experimentally, the H(1) shift being noticeably smaller than predicted (Table 2). This difference may arise because the differences in the hydrogen-bond (O−H···O) angles have not been taken into account in the formalism.[56] Note that the H(2) resonance is broader ($\Delta\nu_{1/2}$ = 220 Hz) than the H(1) ($\Delta\nu_{1/2}$ = 180 Hz) resonance, which is tentatively ascribed to the fact that H(2) sits in a symmetric hydrogen-bond environment with a double minimum, while H(1) sits in an asymmetric bond.[12]

Table 1. Reported Hydrogen-Bond Distances Obtained by X-ray (XRD) and Neutron (ND) Diffraction Method for CsH_2PO_4 in the Paraelectric Phase

methods	d(O(1)−H(1)···O(2))/Å	d(O(3)−H(2)···O(3))/Å
XRD[10]	2.533(5)	2.467(6)
XRD[35]	2.537(7)	2.472(7)
XRD[50]	2.562(6)	2.427(5)
ND[47]	2.538(3)	2.52(2)
ND[48,49]	2.521(5)	2.464(5)

Table 2. Assignment of Hydrogen Bonds in CsH_2PO_4 by ^{1}H and ^{2}H NMR at Room Temperature

		^{1}H δ_{iso}/ppm		^{2}H C_Q/kHz	
hydrogen bonds	distance/Å[10]	measured	estimated[a]	measured	estimated[b]
O(1)−H(1)···O(2)	2.53	10.9	14.5	155	157
O(3)−H(2)···O(3)	2.47	14.3	16.1	118	123

[a]Based on the relationship of chemical shift δ_{iso} and donor-to-acceptor distance (eq 6) using the X-ray data from the literature.[10] [b]Based on the reported linear relationship between the experimental ^{1}H δ_{iso} and ^{2}H C_Q (eq 7).

^{2}H NMR was used to investigate hydrogen bonding further.[34,57−59] The ^{2}H NMR spectrum of CsD_2PO_4 (Figure 3) can be fit with two Pake doublets having slightly different C_Q values (155 and 118 kHz) corresponding to the two different deuterons. Note that a trace amount of D_2O is present, giving rise to the sharp resonance at 4.8 ppm; this sample was freeze-dried rather than being dried under vacuum (the method used to dry the protonated samples). Using the relationship between ^{1}H chemical shift (in ppm) and ^{2}H quadrupole coupling constant (in kHz):[57]

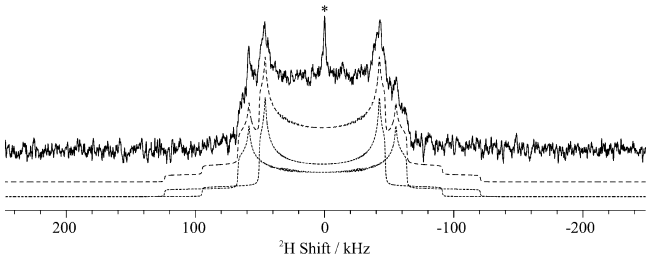

Figure 3. Room-temperature ^{2}H static NMR spectrum of CsD_2PO_4 obtained at 11.7 T. The experimental spectrum is shown as a full line, while the total fit and individual component fit to C_Q = 155 kHz, η_Q = 0.07 for D(1) and C_Q = 118 kHz, η_Q = 0.05 for D(2) are shown with dashed and dotted lines, respectively. The asterisk (*) denotes a trace amount of D_2O at 4.8 ppm.

$$\delta_{iso} = 26.6 - 0.1C_Q \quad (7)$$

the ^{2}H sites with C_Q values of 155 and 118 kHz could be assigned to H(1) and H(2), respectively (Table 2). Furthermore, the estimated C_Q values, calculated with the experimental ^{1}H chemical shifts, are in very good agreement with the measured ^{2}H values (Table 2). Nonzero values of η_Q are observed for both sites, the distortion from axial symmetry being most pronounced for D(1) (η_Q is 0.07 versus 0.05). Axial symmetry is expected for a linear H-bond, and deviations from axial symmetry indicate the presence of either a bent H-bond or librational motion of the deuterons. Note that librational motion results in a reduction of the quadrupole but no change in η_Q; a nonzero value of η_Q will, for example, result from libration in a plane, η_Q = 0.07 corresponding to a libration of ±12° (as determined from simulations of the ^{2}H line shape, performed as a function of libration angle, see Figure S5).[43] The observation of nonzero values of η_Q is consistent with an O−H H-bonding distance that is longer than implied by the crystallographically determined O−O distance and hence is consistent with the explanation for the smaller than predicted (based on the O−O distances) ^{1}H chemical shifts that are observed experimentally. Furthermore, the large value of η_Q for D(1) versus D(2) is consistent with the larger deviation between predicted and experimental ^{1}H chemical shifts.

3.2. Variable-Temperature ^{1}H NMR. Variable-temperature ^{1}H MAS spectra (Figure 4 and Figure S3 with full spectral width) of CsH_2PO_4 show significant temperature dependence in the 39−250 °C temperature range studied. Upon heating, three regions are distinguishable. From room temperature to 195 °C, the signals of the two individual protons in CsH_2PO_4 start to merge and then coalesce above 205 °C to give rise to a resonance with an isotropic chemical shift of 12.3 ppm consistent with a two-site exchange process. Between 215 and 243 °C, the ^{1}H spectra become slightly broader ($\Delta\nu_{1/2}$ = 1600 Hz at 215 °C versus $\Delta\nu_{1/2}$ = 2700 Hz at 243 °C). A loss of spinning side bands in this temperature range is also seen (Figure S3), which (together with the broadening of the isotropic resonance) is ascribed to an interference between the protonic motion and MAS.[58,59] This is consistent with a noticeable increase in motion as the paraelectric−superprotonic phase transition is approached. The phase transition occurs

dx.doi.org/10.1021/jp312410t | J. Phys. Chem. C 2013, 117, 6504−6515

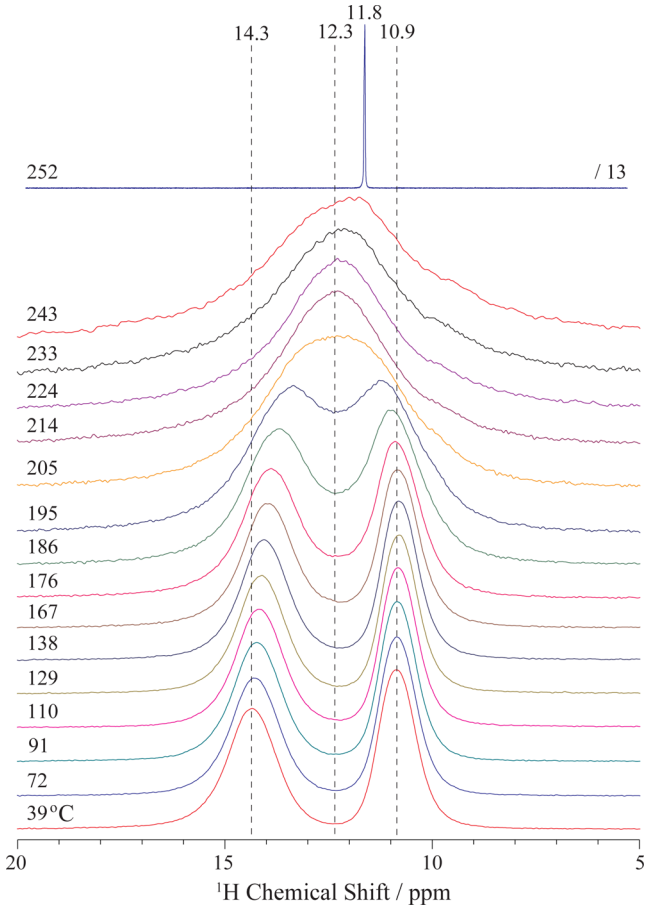

Figure 4. Variable-temperature ^{1}H MAS spectra of CsH_2PO_4 obtained at 11.7 T with a MAS frequency of 14 kHz. The intensity of the peak at 252 °C is scaled down by a factor of 13.

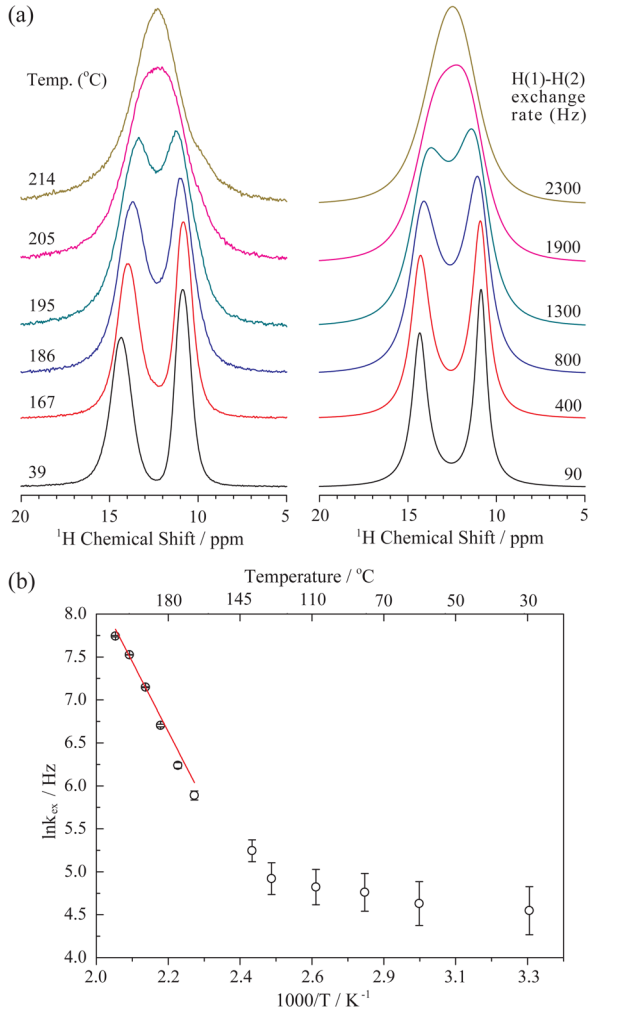

Figure 5. (a) Experimental (left) ^{1}H NMR spectra of CsH_2PO_4 as a function of temperature and simulated (right) ^{1}H line shape assuming a two-site exchange process with rate k_{ex}. Analysis was not performed above 214 °C, because above this temperature, line broadening is ascribed to a second mechanism. (b) Arrhenius plot of the two-site exchange process obtained from NMR. The red line corresponds to the Arrhenius equation least-squares fit with $E_a = 0.70 \pm 0.07$ eV in the high-temperature region (167–214 °C).

above 240 ± 5 °C as measured by NMR, the broad component of the ^{1}H NMR spectrum completely disappearing and leaving a spectrum that is dominated by a single narrow resonance ($\Delta\nu_{1/2}$ = 20 Hz at 11.8 ppm). The observation of a narrow resonance is consistent with the presence of fast diffusive motion of protons in the superprotonic phase as observed in the previous conductivity measurements ($\sigma = 2.2 \times 10^{-2}$ S cm^{-1} at 240 °C[12]). Note that the difference between the reported phase transition temperature (230 ± 2 °C) and that observed here (240 ± 5 °C) must reflect an error in the temperature calibration. We have observed that these calibration errors become larger when closer to the temperature limit of the controller, where higher flows of VT gases are required. It is worth noting that even small differences in the flow rate of bearing, drive, VT gases, and variation in the MAS spinning speed can result in significant changes in sample temperature.

The variable-temperature ^{1}H MAS data from room temperature to 214 °C were fitted to extract the motional exchange rates (k_{ex}) (Figure 5a) by assuming a two-site exchange process. The k_{ex} values were obtained from the following equations[41] where the line shape $g(\omega)$ is given by

$$g(\omega) = \frac{1}{N}\frac{L}{(1 - Lk_{ex})} \tag{8}$$

with

$$L = \sum_{j=1}^{N}\left[i(\omega - \omega_j) - \frac{1}{T_{2j}} + Nk_{ex}\right]^{-1} \tag{9}$$

and N is the number of exchange sites (N = 2 here), T_{2j} is the transverse relaxation time, and ω_j is the resonance frequency of the jth site. A good fit to the experimental data is obtained, indicating slow proton exchange between the two proton sites. The exchange rate at the coalescence temperature (where the two peaks merge) of 205 °C can also be calculated:

$$k_{ex} = \left|\frac{\Omega_\Delta}{2}\right| \tag{10}$$

where Ω_Δ is the chemical shift difference between two different environments,[33] yielding an identical exchange rate ($k_{ex} \simeq 1900$ Hz). A plot of the exchange rate, k_{ex}, versus reciprocal temperature, T^{-1} (Figure 5b), shows that the protonic motion is thermally activated and follows an Arrhenius behavior:

dx.doi.org/10.1021/jp312410t | J. Phys. Chem. C 2013, 117, 6504–6515

$$k_{ex} = Ae^{-E_a/RT} \quad (11)$$

where E_a is the activation energy of the motion. Two different motional mechanisms are clearly apparent below and above ~140 °C and have very different activation energies. The high-temperature protonic motion occurs with an activation energy of 0.70 eV. Given that additional sources of linebroading due to the interference of motion with the removal of linebroadening by MAS become apparent above 214 °C, we also reanalyzed the data, removing the 214 °C data point. This led to a slightly higher activation energy of 0.77 eV, indicating that the measured activation energy of 0.70 eV is only accurate to ±0.07 eV. The measured value is close to the protonic conductivity measurement obtained by AC impedance spectroscopy (0.68 ± 0.02 eV[13]). Variable-temperature ^{2}H static NMR spectra are shown in Figure S4 and reveal very little change up to 200 °C, in agreement with the measured ^{1}H motional frequency (1900 Hz at 205 °C), which will be too slow to affect the ^{2}H one-dimensional line shape (≃100 kHz). A process with a lower activation mechanism is also observed at lower temperature, which, when modeled as a two-site exchange process, yields an activation energy of ~0.05 eV. This may be due to a ^{1}H librational motion or possibly the onset of phosphate ion rotation. It is important to note (as discussed further below) that neither a librational nor phosphate motion should be analyzed by using the two-site exchange model, and thus the determined activation energy can only be taken as an indication that a motional process is present, which appears to have a much lower activation energy.

3.3. ^{1}H Spin–Lattice Relaxation Times versus Temperature: Protonic Motion on the MHz Time Scale. A plot of T_1 versus temperature is given in Figure 6 for two different Larmor frequencies (200 and 500 MHz) and shows that as the temperature is increased, the T_1 (at 500 MHz) gradually decreases from 140 ± 9 s at 37 °C to 1.4 ± 0.2 s at 251 °C. Above 235 °C, an abrupt change of T_1 by more than 1 order of magnitude is observed and is in agreement with the increase in protonic motion in the superprotonic phase.

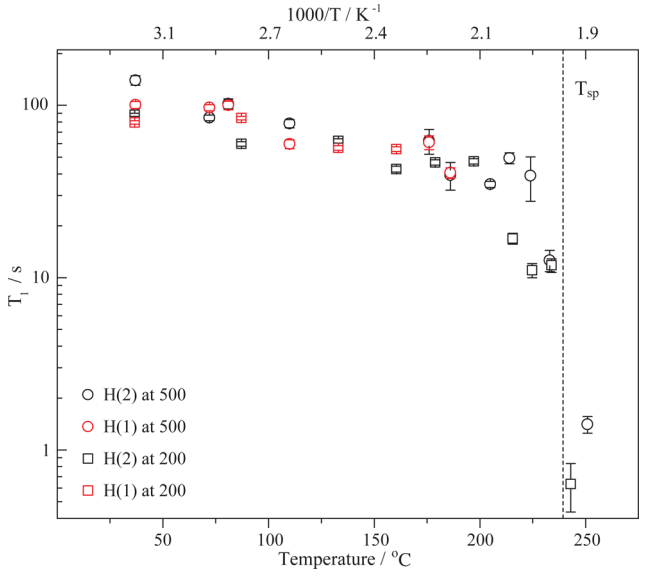

Figure 6. Temperature dependence of the ^{1}H T_1 spin–lattice relaxation times of the two protons in CsH_2PO_4 at ^{1}H Larmor frequencies of 200 and 500 MHz. Independent T_1 measurements for the two protons cannot be made at and above the coalescence temperature. The clear drop in T_1 values above 235 °C, indicated by a dashed line, results from the paraelectric–superprotonic phase transition (T_{sp}). Note that some error bars are smaller than the size of the data points.

The T_1 relaxation is a measure of the time for the spin population to recover to equilibrium after a perturbation and is mediated by fluctuations of the local magnetic fields, as quantified by the correlation time (τ_c) of the motion, with frequencies ($1/\tau_c$) that are on the order of the Larmor frequency, i.e., MHz. A significant contribution to the ^{1}H relaxation mechanism in CsH_2PO_4 comes from the proton homonuclear dipolar interaction. Assuming this mechanism is dominant, then the correlation time of the motion τ_c can be obtained from eq 12:[60−62]

$$\left(\frac{1}{T_1}\right)_{dipolar} = \frac{3}{5}\left(\frac{\mu_0}{4\pi}\right)^2 \gamma_H^4 \hbar^2 I(I+1)\left(\sum_i \frac{1}{r_i^6}\right) \times \left[\frac{\tau_c}{1+\omega_0^2\tau_c^2} + \frac{4\tau_c}{1+4\omega_0^2\tau_c^2}\right] \quad (12)$$

by summing over all of the ^{1}H−^{1}H internuclear distances (r_i) extracted from the crystal structure (ω_0 is the ^{1}H Larmor frequency and τ_c is the correlation time of the motion). Note that the prefactor in eq 12 is controlled by the second moment (M_2), which is proportional to the square of the dipolar coupling constant d_{HH} as defined in eq 13:

$$d_{HH} = -\left(\frac{\mu_0}{4\pi}\right)\frac{\gamma_H^2\hbar}{r_i^3} \quad (13)$$

The value of M_2 (2.6×10^8 Hz^2) calculated from the room-temperature crystallographic data[10] was used to predict the T_1 values at all temperatures as to the best of our knowledge there are no accurate crystallographic data available for CsH_2PO_4 above room temperature. The correlation times extracted with this approach show a significant field dependence, which has no obvious physical basis. To account for this field dependence, a second term, which includes interactions whose magnitude (in frequency units) scales with the field (i.e., dipolar interactions involving paramagnetic impurities[63] and the ^{1}H CSA), is introduced. The modified equation is shown below:

$$\frac{1}{T_1} = \left(\frac{1}{T_1}\right)_{dipolar} + \left(\frac{1}{T_1}\right)_{field\text{-}dependent}$$

$$= \frac{3}{5}\left(\frac{\mu_0}{4\pi}\right)^2 \gamma_H^4 \hbar^2 I(I+1)\left(\sum_i \frac{1}{r_i^6}\right)\left[\frac{\tau_c}{1+\omega_0^2\tau_c^2} + \frac{4\tau_c}{1+4\omega_0^2\tau_c^2}\right] + P^2\omega_0^2\left[\frac{\tau_c}{1+\omega_0^2\tau_c^2}\right] \quad (14)$$

where P is an empirical scaling factor that incorporates the CSA and paramagnetic interactions. A series of plots of log T_1 versus log τ_c were generated by using eq 14, varying P so as to yield the closest correspondences between the correlation times extracted from the two data sets acquired at two fields. The most consistent set is shown in Figure 7a and corresponds to a field-dependent factor $P^2\omega_0^2$ of 4.2×10^9 Hz^2. Assuming that $P^2\omega_0^2$ is dominated by the ^{1}H CSA, this corresponds to a value of ~20 ppm, which is of the same order of magnitude as many reported ^{1}H CSAs for OH protons.[64,65] Figure 7b displays the

dx.doi.org/10.1021/jp312410t | J. Phys. Chem. C 2013, 117, 6504−6515

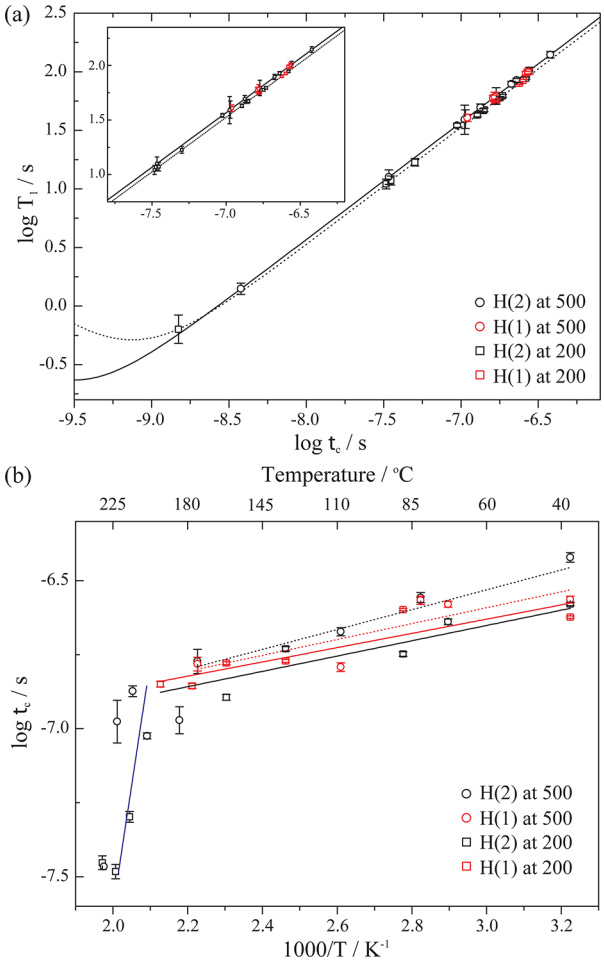

Figure 7. (a) A plot of log T_1 versus log τ_c, calculated by using eq 14, Larmor frequencies of 500 and 200 MHz and a value for $P^2\omega_0^2$ of 4.2 × 10^9 Hz^2. The experimental data points are shown as open circles and squares for the 500 and 200 MHz fields, respectively. The solid and dotted lines represent the plots of eq 14 for the 500 and 200 MHz fields, respectively, and the inset shows the experimental data points with larger T_1 values (with error bars). (b) Arrhenius plot of the ^{1}H T_1 spin−lattice relaxation times obtained from NMR at 500 and 200 MHz in the 37−205 °C temperature range. Fits are shown by red lines for H(1) and black lines for H(2), respectively. A (blue) line with a slope corresponding to the activation energy (0.70 ± 0.07 eV) determined from the high-temperature ^{1}H 1D data is shown for comparison.

temperature dependence of the correlation times (τ_c) at the two different magnetic fields. Although the scatter of the data in the high-temperature (180−225 °C) regime is large, the data are consistent with the activation energy (0.70 ± 0.07 eV) determined from the line shape analysis of 1D spectra. The activation energy of the process occurring at lower temperatures is much lower, and using the model developed above, we obtain a very similar and small activation energy for the motion of both protons of CsH_2PO_4 in the 37−205 °C temperature range of between 0.01 and 0.04 eV. (Note that in a system where the T_1's are long, proton spin-diffusion will result in an equilibration of the T_1 values of the different species, and thus both protons likely detect the same motional processes.) The measured activation energies are similar in magnitude to that determined in the 1D ^{1}H spectra. However, as discussed previously, analysis of the data within this Bloembergen, Purcell and Pound model effectively assumes isotropic motion, which is not appropriate for a local librational motion. Thus, again the measured activation energies should simply be taken as an indication that low activation processes exist before the onset of the proton two-site exchange. Correlation times of 1.1 and 3.7 × 10^{-9} s at approximately 246 °C are extracted for the 200 and 500 MHz data, respectively, in the superprotonic phase, the differences in the two measurements presumably reflecting small differences in temperature.

3.4. Variable-Temperature ^{31}P MAS NMR. The variable-temperature ^{31}P MAS NMR spectra are shown in Figure 8 and

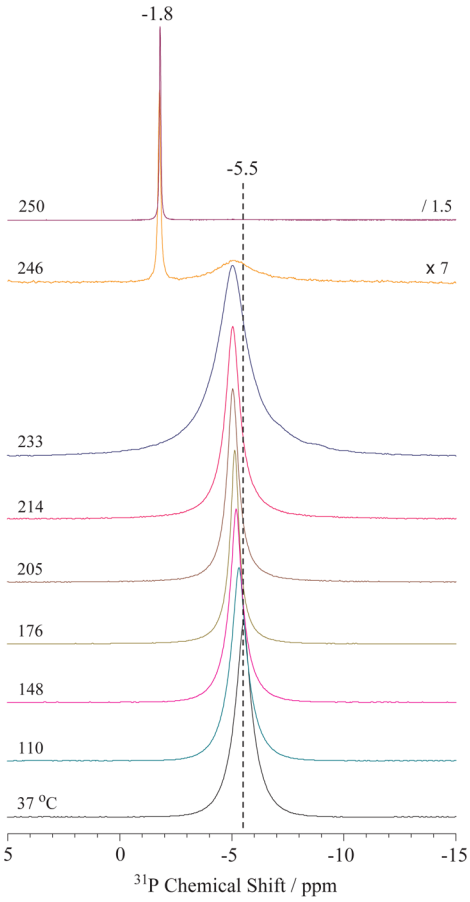

Figure 8. Variable-temperature ^{31}P MAS NMR spectra of CsH_2PO_4. The ^{31}P isotropic shift is labeled for both the paraelectric (below 246 °C) and superprotonic (at and above 246 °C) phases. Full ^{31}P spectra with spinning side bands are shown in Figure S6.

Figure S6 (full spectral width). The extracted ^{31}P isotropic chemical shifts (Table 3) are consistent with the values obtained from the ^{31}P chemical shift anisotropy (CSA) patterns (vide infra). One crystallographic ^{31}P site is observed in agreement with the crystal structure.[10,35] In the paraelectric phase, the ^{31}P signal shows a continuous small shift to higher frequencies (−5.5 ppm at room temperature to −5.0 ppm at 214 °C). This is consistent with the small displacement of the atomic position of phosphorus as observed previously in the paraelectric phase,[47] which is likely caused by the onset of motion. Concomitantly, the ^{31}P MAS line width ($\Delta\nu_{1/2}$) significantly increases above 205 °C, from 127 Hz (205 °C) to 335 Hz (233 °C), in a way that is analogous to the broadening already observed for the ^{1}H MAS spectra (Figure 4); we similarly ascribe this broadening to the interference of the proton motion with the ability of MAS to remove the ^{31}P−^{1}H dipolar coupling. At 246 °C, in addition to the peak at −5 ppm,

dx.doi.org/10.1021/jp312410t | J. Phys. Chem. C 2013, 117, 6504−6515

Table 3. ^{31}P NMR Variable-Temperature NMR Parameters of CsH_2PO_4 Extracted from the Fits of the ^{31}P Static Spin–Echo Experiments Obtained at 8.45 T (Figure 9)[a]

	with ^{1}H decoupling			without ^{1}H decoupling		
T/°C[b]	δ_{iso}/ppm	δ_{aniso}/ppm	η	δ_{iso}/ppm	δ_{aniso}/ppm	η
21	−5.6	−46	0.87			
180	−4.3	−46	0.91		−[c]	
200	−4.4	−46	0.92			
215	−5.9	−45	0.90	−6.5	−43	0.99
220	−1.7[d]			−1.7[d]		
	−2.5[d]	−55	1.00	−2.9[d]	−52.1	0.74
230	−1.7[e]			−1.7[e]		

[a]Simulations were performed with DMFit.[39] [b]Temperature not calibrated for static experiment. [c]Not determined due to the significant ^{1}H–^{31}P dipolar interactions. [d]Two component fit: a sharper resonance described by a Gaussian/Lorentzian and one broadened by the CSA. [e]Obtained by spectral deconvolution using a Gaussian/Lorentzian.

a second, much narrower, peak is observed at higher frequency (−1.8 ppm), which is attributed to a rapidly rotating phosphate group in the superprotonic phase. It is noteworthy that spinning sidebands of ^{31}P MAS NMR spectra remain throughout the whole temperature range of the paraelectric phase (Figure S6), indicating a local motion, which should be contrasted to the observations in the proton MAS spectra.

3.5. Variable-Temperature ^{31}P Static NMR. The variable-temperature ^{31}P NMR static spectra (obtained with ^{1}H decoupling) are shown in Figure 9a and show a typical pattern arising from CSA. Fitting of the line shape at room temperature yields CSA principal components in agreement with reported values in the literature (Figure 9 and Table 3).[13,66] The line shape remains almost identical up to 215 °C, and is thus in apparent disagreement with the previously reported single crystal static ^{31}P spectra of CsH_2PO_4[13] where broadening and coalescence were observed. At 220 °C, a narrow resonance is observed, in addition to a weak residual signal from the broader component, the narrowing being ascribed to the fast reorientation of the tetrahedral phosphate ion in the superprotonic phase. Although the line width of the resonance ($\Delta\nu_{1/2}$ = 1.1 kHz) is reduced, the residual broadening suggests that, although the phosphate ion is mobile, the motion of the phosphate is not liquid-like. The apparent phase transition temperature seen in the ^{31}P static NMR is now close to a measured temperature of 220 °C, which is lower than the reported transition (230 ± 2 °C). This discrepancy is largely ascribed to the fact that the measurements were done in the absence of MAS, while the calibration was performed under MAS. The coexistence of signals from both the paraelectric and the superprotonic phase at this temperature is ascribed to a temperature gradient in the sample.

The variable-temperature ^{31}P spectra obtained without ^{1}H decoupling are shown in Figure 9b. Although the room-temperature line shape is clearly dominated by both ^{31}P CSA and ^{1}H–^{31}P dipolar interactions, as the temperature is increased, motional averaging of the ^{1}H–^{31}P dipolar coupling is observed yielding at approximately 215 °C (i.e., close to the phase transition) a line shape that is almost entirely dominated by the ^{31}P CSA interaction (see Figure 9a and b at 215 °C). This ^{1}H self-decoupled ^{31}P spectrum results from the fast protonic motions as observed in the ^{1}H NMR data. Note that small differences are still observed between the ^{1}H decoupled and one-pulse ^{31}P spectra without ^{1}H decoupling, indicating

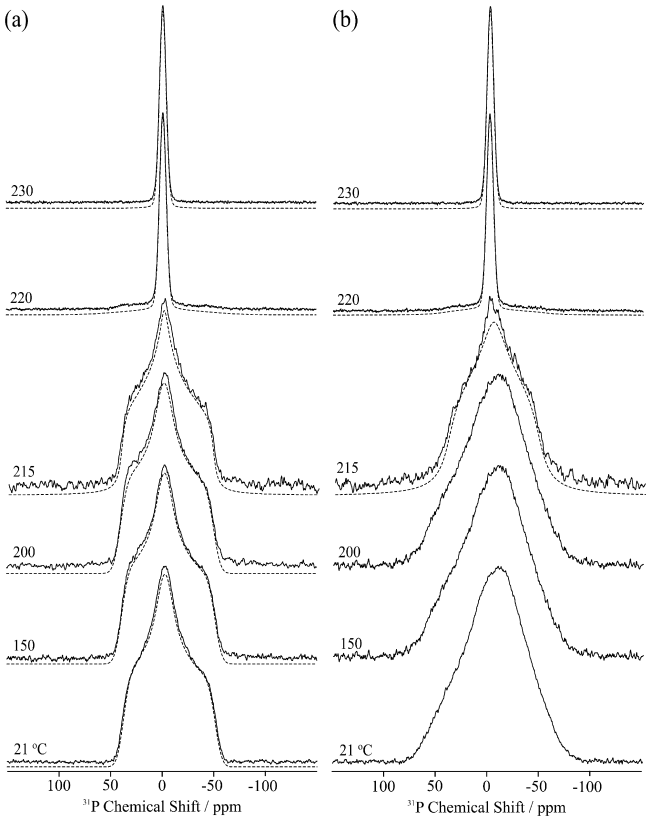

Figure 9. Variable-temperature ^{31}P static NMR spectra of CsH_2PO_4 (a) with ^{1}H decoupling, and (b) without ^{1}H decoupling at 8.45 T. The phase transition is observed at an apparent temperature of 220 °C. Dashed lines show the best fit simulations assuming ^{31}P CSA interactions only and both ^{31}P CSA and ^{1}H–^{31}P dipolar interactions in (a) and (b), respectively. The extracted NMR parameters are summarized in Table 3. Simulations were performed with DMFit.[39]

that residual heteronuclear dipolar interactions persist close to the phase transformation (as explored further in the Supporting Information).

3.6. ^{31}P Spin–Lattice and Spin–Spin Relaxation Times versus Temperature. The temperature dependence of both ^{31}P T_1 relaxation times and the T_2* relaxation times (defined as

$$T_2^* = \frac{1}{\pi\Delta} \quad (15)$$

where Δ denotes the line width) is shown in Figure 10. The ^{31}P T_1 gradually decreases from 543 ± 7 s at room temperature to 301 ± 3 s at 233 °C. An abrupt drop in the T_1 by more than 2 orders of magnitude (to 1.8 ± 0.3 s) is observed at 246 °C. This drop is in agreement with the paraelectric–superprotonic phase transition. Examining the T_2* relaxation times as a function of temperature, the reverse behavior is observed with a sharp increase at the paraelectric–superprotonic phase transition (from 3.2 ms at 186 °C to 19.8 ms at 249 °C).

Assuming that ^{31}P relaxation is dominated by the ^{1}H–^{31}P heteronuclear dipolar and ^{31}P CSA interactions (see the Supporting Information for more discussion and Figures S8,S9), two distinct activation energies of 0.019 ± 0.001 eV (72–205 °C) and 0.047 ± 0.005 eV (214–233 °C), respectively, are determined (Table 4). These are noticeably lower than those extracted from the ^{1}H MAS data. Of note, in the superprotonic phase, a correlation time of $(1.3–1.7) \times 10^{-8}$ s at approximately 246 °C is extracted. Given that the ^{31}P CSA

dx.doi.org/10.1021/jp312410t | J. Phys. Chem. C 2013, 117, 6504–6515

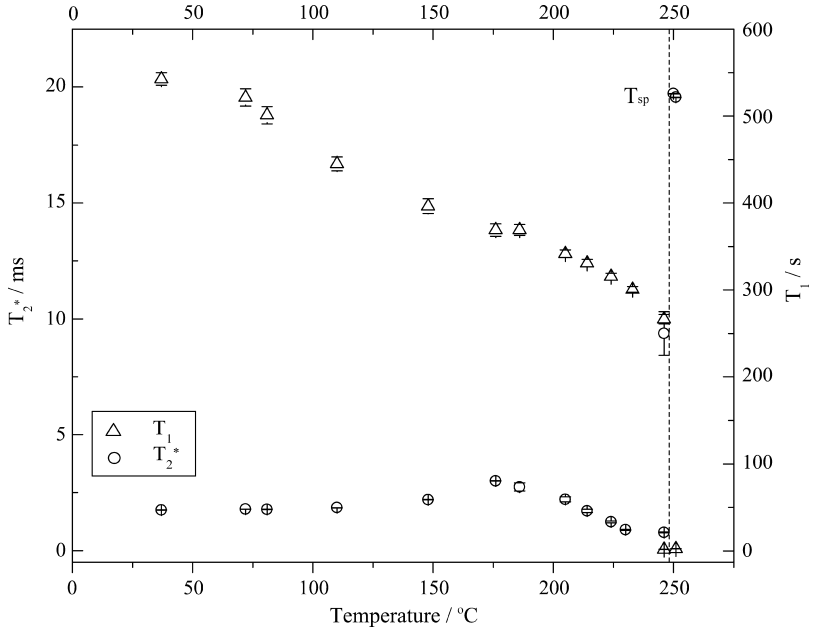

Figure 10. Temperature dependence of ^{31}P T_1 (△) and T_2* (○) relaxation times of CsH_2PO_4 measured at a field strength of 11.7 T (500 MHz). The dashed line denotes the paraelectric−superprotonic phase transition that occurs at T_{sp} = 246 °C.

Table 4. ^1H and ^{31}P Motional Frequencies Obtained by the Different NMR Techniques

nuclei	method and model used to extract data	T range/°C	E_a/eV	motional frequency/Hz
^1H	two-site exchange	167−214	0.70 ± 0.07	1900 (205 °C)
	two-site exchange	39−129	~0.05[a]	
	interference with MAS	approx. 230		~14k
	T_1 analysis	37−205	0.02 ± 0.01[a]	
		246−251		(2.7−8.9) × 10^8[b]
^{31}P	T_1 analysis	72−205	0.019 ± 0.001[a]	
		214−233	0.047 ± 0.002	
		246−251		(0.6−0.8) × 10^8[c]

[a]Note that the model used to fit these data may not apply in this temperature range. [b]Obtained at both 200 and 500 MHz. [c]Obtained at 500 MHz.

was not found to be sensitive to motion in the paraelectric phase, we also reanalyzed the data by assuming that ^{31}P T_1 relaxation is only affected by the ^1H−^{31}P heteronuclear dipolar interaction, but activation energies of a similar magnitude were extracted (see Figure S9 and discussion in the Supporting Information). The effect of different correlation times for proton translational and phosphate reorientational motion will be discussed in a subsequent paper.

4. DISCUSSION

Various motions of CsH_2PO_4 observed by the different NMR experiments are summarized in Table 4. Analysis of the two-site exchange process obtained from our ^1H MAS NMR data yields an activation energy that is in good agreement with a reported value from a conductivity measurement[13] and is ascribed to the long-range protonic motion in this compound. After the coalescence of the two ^1H resonances, caused by the two-site exchange process, the ^1H resonances actually broaden, rather than sharpen, as the paraelectric−superionic phase transition is approached. The ^1H spinning side bands also broaden and disappear in this temperature range (Figure S3). We ascribe this to the interference between MAS (ν_r = 14 kHz) and motion. Simulations of static ^{31}P NMR data showed that ^1H−^1H and ^1H−^{31}P dipolar interactions are significantly reduced in this temperature regime (Figure S7), also consistent with motion in the kHz range.

A second, lower energy activation process is also observed. This motional process has a much shorter correlation time, because it is responsible for the reduction in T_1 times, which requires motion on the MHz time scale. On this basis, we tentatively ascribe the reduction in T_1 times of both the ^1H and the ^{31}P to a librational process, which is also consistent with the proposal made on the basis of the ^2H quadrupolar parameters. Librations involving hydrogen-bonded protons are commonly reported in proton conducting systems,[16] and they may reduce the overall energy barrier for proton hopping. This idea is supported by a recent high-temperature PFG/QENS study of CsH_2PO_4 in the superprotonic phase,[17] which also indicated that protonic motions are comprised of two motional processes, translation and libration. The low proton conductivity in the paraelectric phase (8.5 × 10^{-6} S cm^{-1} at 223 °C[12]), 4 orders of magnitude lower than that of the superprotonic phase, further supports the proposal that the high frequency motions are localized. The motional time scales are 5 orders of magnitude higher in the superprotonic phase, on the basis of a comparison between the frequencies measured by two-site exchange and the ^1H T_1's (Table 4). Of interest, the motional frequency extracted from the ^1H T_1 value (2.7 × 10^8 Hz) is of the same order of magnitude as the ^{31}P T_1 ((0.6−0.8)

dx.doi.org/10.1021/jp312410t | J. Phys. Chem. C 2013, 117, 6504−6515

$\times 10^8$ Hz), for the data measured at the same time and temperature, with the same MAS probe. The slightly larger value for protonic motion is in agreement with reported computational studies.[19] However, these values should be treated with caution because of the difficulty of separating the different relaxation mechanisms with such a limited data set and the assumptions made in the T_1 analyses. More detailed studies are required over a wider range of temperatures in the superprotonic phase at multiple field strengths.

In contrast to the ^{1}H NMR spectra, the ^{31}P MAS and static line shapes do not vary noticeably in the paraelectric phase. Of particular note, the ^{1}H-decoupled ^{31}P static spectra (Figure 9a) clearly show that the CSA is not averaged by any motion that is present in the paraelectric phase. This is in apparent contrast to earlier ^{31}P single crystal NMR studies where an estimate of the phosphate reorientation of 25 kHz (at 207 °C)[13] was done. Isotropic reorientation at this rate should have averaged out the observed CSA pattern (δ_{aniso} = 46 ppm, ~7 kHz at 8.45 T, Table 3). Two explanations are possible: either the motional frequency of the phosphate rotation is lower than ~7 kHz (i.e., slower than reported values[13]) or the ^{31}P CSA is not sensitive to the reorientation of phosphate ions. The CSA is likely to result from the asymmetry of H-bonding to the four oxygen atoms of the phosphate ions, and thus rotations of the phosphate units do not remove this asymmetry (i.e., the phosphate unit still feels the effect of the local asymmetry in bonding). Note that the loss of the ^{31}P CSA line shape above the phase transition is ascribed to the isotropic motion that occurs in the cubic phase. On the basis of our current data, it is not possible to determine whether protonic motion facilitates phosphate rotation or whether the onset of phosphate rotation leads to faster motion of protons, because we have still not determined the time scale of the phosphate rotation. The combination of our ^{1}H NMR results (1.9 kHz at 205 °C) and the earlier ^{31}P single crystal data (25 kHz at 207 °C)[13] suggests that it is the latter, but further experiments are still required to explore this further. To this end, ^{17}O NMR experiments are ongoing to directly investigate the phosphate ion rotation.

5. CONCLUSIONS

^{1}H, ^{2}H, and ^{31}P NMR spectroscopy has been applied to provide a more detailed understanding of proton conduction of CsH_2PO_4, focusing on the paraelectric phase. Two proton (deuteron) environments are identified with very different chemical shifts and quadrupolar parameters. The NMR parameters of the proton/deuteron in the asymmetric H-bond are consistent with small deviations in the linearity of the O−H···O H-bond resulting in a H-bonding distance that is longer than implied by the O−O distance derived from the crystal structure reported in the literature.[10] A librational O−H(D) motion also accounts for these observations; that is, the displacement of the H/D atom from the O−O interatomic vector is dynamic in origin. Deviations between NMR parameters calculated from the crystal structure and the measured values are smaller for the symmetric H-bond, suggesting that this bond is closer to being linear. Two types of protonic motion are identified corresponding to translational and librational motions, both motions having been observed previously in the superprotonic phase.[17] These motions are cooperative, and this librational motion may reduce an overall energy barrier for proton hopping. To probe the motion of the phosphate ions, various ^{31}P NMR measurements have been performed as a function of temperature. The ^{31}P spectra are sensitive to the protonic motion, but quantification of the rotational frequency of the phosphate ions proved difficult, because no significant change in the ^{31}P CSA was observed in the paraelectric phase. The results suggest that the ^{31}P CSA is a measure of the asymmetry in proton coordination to the phosphate ion and is thus largely insensitive to the reorientation of the phosphate ions in the paraelectric phase. However, in the superprotonic phase, phosphate rotation coupled with fast motion of the protons does result in removal of the CSA. A significant increase of more than 5 orders of magnitude in the correlation time for the protonic motion was observed on heating from just below the phase transition (205 °C) to just above, as measured by ^{1}H NMR.

■ ASSOCIATED CONTENT

Supporting Information

PXRD patterns of CsH_2PO_4 and CsD_2PO_4 (Figure S1), full spectral width ^{1}H ultrafast MAS spectrum of CsH_2PO_4 (Figure S2), full spectral width variable-temperature ^{1}H MAS NMR spectra of CsH_2PO_4 (Figure S3), additional discussion on the variable-temperature ^{2}H NMR static spectra (Figure S4), simulations of ^{2}H static line shape to show the effect of the librational motion on the line shape (Figure S5), full spectral width variable-temperature ^{31}P MAS NMR spectra of CsH_2PO_4 (Figure S6), additional discussion on the simulations of the effect of protonic motions on the ^{31}P static NMR data (Figure S7), analysis of ^{31}P spin−lattice relaxation times (Figure S8), and plots of ^{31}P log T_1 versus log τ_c for the different models (Figure S9). This material is available free of charge via the Internet at http://pubs.acs.org.

■ AUTHOR INFORMATION

Corresponding Author

*Phone: +44 (0)1223 336509. Fax: +44 (0)1223 336509. E-mail: cpg27@cam.ac.uk.

Notes

The authors declare no competing financial interest.

■ ACKNOWLEDGMENTS

G.K., F.B., and C.P.G. thank the NSF via grant DMR0804737, and the New York State Foundation for Science, Technology and Innovation via a NYSTAR award. F.B. also thanks the French foreign office for a post doctoral Lavoisier fellowship 2007-2008 (grant no. 530227G) and the EU Marie Curie actions FP7 for an International Incoming fellowship (grant no. 275212) for financial support. C.P.G. and G.K. thank the European Research Council for an Advanced Fellowship. Y.-Y.H. acknowledges support from a Newton International Fellowship, which is run by The British Academy and the Royal Society. We thank Prof. Gillian R. Goward for useful discussions, and Dr. John M. Griffin, Dr. Michal Leskes, and Ben Yunxu Zhu for valuable discussions about ^{2}H, ^{31}P, and ^{1}H NMR simulations. We also thank Dr. Lisa A. Cowan and Prof. Sossina M. Haile for providing a sample of CsH_2PO_4 and fruitful discussions.

■ REFERENCES

(1) Norby, T. The Promise of Protonics. *Nature* **2001**, *410*, 877−878.

(2) Norby, T. Solid-State Protonic Conductors: Principles, Properties, Progress and Prospects. *Solid State Ionics* **1999**, *125*, 1−11.

(3) Wachsman, E. D.; Lee, K. T. Lowering the Temperature of Solid Oxide Fuel Cells. *Science* **2011**, *334*, 935−939.

(4) Haile, S. M.; Boysen, D. A.; Chisholm, C. R. I.; Merle, R. B. Solid Acids as Fuel Cell Electrolytes. *Nature* **2001**, *410*, 910−913.
(5) Boysen, D. A.; Uda, T.; Chisholm, C. R. I.; Haile, S. M. High-Performance Solid Acid Fuel Cells Through Humidity Stabilization. *Science* **2004**, *303*, 68−70.
(6) Uda, T.; Haile, S. M. Thin-Membrane Solid-Acid Fuel Cell. *Electrochem. Solid-State Lett.* **2005**, *8*, A245−A246.
(7) Varga, Á.; Brunelli, N. A.; Louie, M. W.; Giapis, K. P.; Haile, S. M. Composite Nanostructured Solid-acid Fuel-cell Electrodes via Electrospray Deposition. *J. Mater. Chem.* **2010**, *20*, 6309−6315.
(8) Song-yul, O.; Evan, K. I.; Van, H. N.; Go, K.; Hiroyuki, M.; Mototsugu, S.; Atsunori, M. Mechanochemically Synthesized CsH_2PO_4-$H_3PW_{12}O_{40}$ Composites as Proton-conducting Electrolytes for Fuel Cell Systems in a Dry Atmosphere. *Sci. Technol. Adv. Mater.* **2011**, *12*, 034402.
(9) Otomo, J.; Tamaki, T.; Nishida, S.; Wang, S.; Ogura, M.; Kobayashi, T.; Wen, C.-J.; Nagamoto, H.; Takahashi, H. Effect of Water Vapor on Proton Conduction of Cesium Dihydrogen Phosphate and Application to Intermediate Temperature Fuel Cells. *J. Appl. Electrochem.* **2005**, *35*, 865−870.
(10) Preisinger, A.; Mereiter, K.; Bronowska, W. The Phase Transition of CsH_2PO_4 (CDP) at 505 K. *Mater. Sci. Forum* **1994**, *166*, 511−516.
(11) Botez, C. E.; Hermosillo, J. D.; Zhang, J.; Qian, J.; Zhao, Y.; Majzlan, J.; Chianelli, R. R.; Pantea, C. High-temperature Phase Transitions in CsH_2PO_4 under Ambient and High-pressure Conditions: A Synchrotron X-ray Diffraction Study. *J. Chem. Phys.* **2007**, *127*, 194701.
(12) Haile, S. M.; Chisholm, C. R. I.; Sasaki, K.; Boysen, D. A.; Uda, T. Solid Acid Proton Conductors: from Laboratory Curiosities to Fuel Cell Electrolytes. *Faraday Discuss.* **2007**, *134*, 17−39.
(13) Yamada, K.; Sagara, T.; Yamane, Y.; Ohki, H.; Okuda, T. Superprotonic Conductor CsH_2PO_4 Studied by ^1H, ^{31}P NMR and X-ray Diffraction. *Solid State Ionics* **2004**, *175*, 557−562.
(14) Baranov, A. I. Crystals with Disordered Hydrogen-bond Networks and Superprotonic Conductivity. Review. *Crystallogr. Rep.* **2003**, *48*, 1012−1037.
(15) Otomo, J.; Minagawa, N.; Wen, C.-J.; Eguchi, K.; Takahashi, H. Protonic Conduction of CsH_2PO_4 and Its Composite with Silica in Dry and Humid Atmospheres. *Solid State Ionics* **2003**, *156*, 357−369.
(16) Colomban, P. *Proton Conductors*; Cambridge University Press: New York, 1992.
(17) Ishikawa, A.; Maekawa, H.; Yamamura, T.; Kawakita, Y.; Shibata, K.; Kawai, M. Proton Dynamics of CsH_2PO_4 Studied by Quasi-elastic Neutron Scattering and PFG-NMR. *Solid State Ionics* **2008**, *179*, 2345−2349.
(18) Traer, J. W.; Soo, K. J.; Vijayakumar, M.; Goward, G. R. Elucidating the Time Scale and Geometry of Phosphate and Phosphonate Rotation in Solid Acid Electrolytes Using Multinuclear NMR. *J. Phys. Chem. C* **2011**, *115*, 6064−6072.
(19) Lee, H.-S.; Tuckerman, M. E. The Structure and Proton Transport Mechanisms in the Superprotonic Phase of CsH_2PO_4: An Ab Initio Molecular Dynamics Study. *J. Phys. Chem. C* **2008**, *112*, 9917−9930.
(20) Belushkin, A. V.; David, W. I. F.; Ibberson, R. M.; Shuvalov, L. A. High-resolution Neutron Powder Diffraction Studies of the Structure of $CsDSO_4$. *Acta Crystallogr., Sect. B* **1991**, *47*, 161−166.
(21) Belushkin, A. V.; Carlile, C. J.; Shuvalov, L. A. The Diffusion of Protons in the Superionic Conductor $CsHSO_4$ by Quasielastic Neutron Scattering. *J. Phys.: Condens. Matter* **1992**, *4*, 389−398.
(22) Damyanovich, A.; Pintar, M. M.; Blinc, R.; Slak, J. Proton Pseudoglass-to-fast-ion-conductor Phase Transition in $CsHSO_4$. *Phys. Rev. B* **1997**, *56*, 7942−7946.
(23) Münch, W.; Kreuer, K. D.; Traub, U.; Maier, J. Proton Transfer in the Three-dimensional Hydrogen Bond Network of the High Temperature Phase of $CsHSO_4$: A Molecular Dynamics Study. *J. Mol. Struct.* **1996**, *381*, 1−8.
(24) Münch, W.; Kreuer, K. D.; Traub, U.; Maier, J. A Molecular Dynamics Study of the High Proton Conducting Phase of $CsHSO_4$. *Solid State Ionics* **1995**, *77*, 10−14.
(25) Chisholm, C. R. I.; Jang, Y. H.; Haile, S. M.; Goddard, W. A., III. Superprotonic Phase Transition of $CsHSO_4$: A Molecular Dynamics Simulation Study. *Phys. Rev. B* **2005**, *72*, 134103.
(26) Zetterström, P.; Belushkin, A. V.; McGreevy, R. L.; Shuvalov, L. A. Structure and Proton Conduction in $CsDSO_4$. *Solid State Ionics* **1999**, *116*, 321−329.
(27) Suzuki, K.; Hayashi, S. ^1H NMR Study of Proton Dynamics in the Inorganic Solid Acid $Rb_3H(SO_4)_2$. *Phys. Rev. B* **2006**, *73*, 024305.
(28) Hayashi, S.; Mizuno, M. Proton Dynamics in $Cs_2(HSO_4)$-(H_2PO_4) Studied by ^1H NMR. *Solid State Ionics* **2005**, *176*, 745−754.
(29) Suzuki, K.; Hayashi, S. Proton Dynamics in $Cs_3(HSO_4)_2(HPO_4)$ Studied by ^1H NMR. *Solid State Ionics* **2006**, *177*, 2873−2880.
(30) Mantsch, H. H.; Saito, H.; Smith, I. C. P. Deuterium Magnetic Resonance, Applications in Chemistry, Physics and Biology. *Prog. Nucl. Magn. Reson. Spectrosc.* **1977**, *11*, 211−272.
(31) Jelinski, L. W. Solid State Deuterium NMR Studies of Polymer Chain Dynamics. *Annu. Rev. Mater. Sci.* **1985**, *15*, 359−377.
(32) Chandrakumar, N.; Fluck, E.; Günther, H. *Spin-1 NMR*; Springer: New York, 1996.
(33) Levitt, M. *Spin Dynamics: Basics of Nuclear Magnetic Resonance*; Wiley: New York, 2008.
(34) Duer, M. J. *Introduction to Solid-state NMR Spectroscopy*; Blackwell: Cambridge, MA, 2004.
(35) Matsunaga, H.; Itoh, K.; Nakamura, E. X-Ray Structural Study of Ferroelectric Cesium Dihydrogen Phosphate at Room Temperature. *J. Phys. Soc. Jpn.* **1980**, *48*, 2011−2014.
(36) Beckmann, P. A.; Dybowski, C. A Thermometer for Nonspinning Solid-State NMR Spectroscopy. *J. Magn. Reson.* **2000**, *146*, 379−380.
(37) Bielecki, A.; Burum, D. P. Temperature Dependence of ^{207}Pb MAS Spectra of Solid Lead Nitrate. An Accurate, Sensitive Thermometer for Variable-Temperature MAS. *J. Magn. Reson., Ser. A* **1995**, *116*, 215−220.
(38) van Beek, J. D. matNMR: A Flexible Toolbox for Processing, Analyzing and Visualizing Magnetic Resonance Data in Matlab. *J. Magn. Reson.* **2007**, *187*, 19−26.
(39) Massiot, D.; Fayon, F.; Capron, M.; King, I.; Le Calvé, S.; Alonso, B.; Durand, J.-O.; Bujoli, B.; Gan, Z.; Hoatson, G. Modelling One- and Two-dimensional Solid-state NMR Spectra. *Magn. Reson. Chem.* **2002**, *40*, 70−76.
(40) Veshtort, M.; Griffin, R. G. SPINEVOLUTION: A Powerful Tool for the Simulation of Solid and Liquid State NMR Experiments. *J. Magn. Reson.* **2006**, *178*, 248−282.
(41) Mehring, M. *Principles of High Resolution NMR Spectroscopy in Solids*, 2nd ed.; Springer-Verlag: Berlin, 1983.
(42) Bak, M.; Rasmussen, J. T.; Nielsen, N. C. SIMPSON: A General Simulation Program for Solid-state NMR Spectroscopy. *J. Magn. Reson.* **2000**, *147*, 296−330.
(43) Macho, V.; Brombacher, L.; Spiess, H. W. The NMR-WEBLAB: An Internet Approach to NMR Lineshape Analysis. *Appl. Magn. Reson.* **2001**, *20*, 405−432.
(44) Pyykkö, P. Year-2008 Nuclear Quadrupole Moments. *Mol. Phys.* **2008**, *106*, 1965−1974.
(45) Boyson, D. A.; Haile, S. M.; Liu, H.; Secco, R. A. High-Temperature Behavior of CsH_2PO_4 under Both Ambient and High Pressure Conditions. *Chem. Mater.* **2003**, *15*, 727−736.
(46) Yesinowski, J. P.; Eckert, H.; Rossman, G. R. Characterization of Hydrous Species in Minerals by High-speed Proton MAS-NMR. *J. Am. Chem. Soc.* **1988**, *110*, 1367−1375.
(47) Itoh, K.; Hagiwara, T.; Nakamura, E. Order-Disorder Type Phase Transition in Ferroelectric CsD_2PO_4 Studied by X-Ray Structure Analysis. *J. Phys. Soc. Jpn.* **1983**, *52*, 2626−2629.
(48) Nelmes, R. J.; Choudhary, R. N. P. Structural Studies of the Monoclinic Dihydrogen Phosphates: A Neutron-diffraction Study of Paraelectric CsH_2PO_4. *Solid State Commun.* **1978**, *26*, 823−826.

(49) Choudhary, R. N. P.; Nelmes, R. J. A Structural Study of CsH_2PO_4 in the Paraelectric Phase. *Ferroelectrics* **1978**, *21*, 443−444.
(50) Uesu, Y.; Kobayashi, J. Crystal Structure and Ferroelectricity of Cesium Dihydrogen Phosphate CsH_2PO_4. *Phys. Status Solidi A* **1976**, *34*, 475−481.
(51) Iwata, Y.; Deguchi, K.; Mitani, S.; Shibuya, I.; Onodera, Y.; Nakamura, E. A Neutron Diffraction Study on the Deuteration Effect in CsH_2PO_4 Crystal. *J. Phys. Soc. Jpn.* **1994**, *63*, 4044−4050.
(52) Iwata, Y.; Koyano, N.; Shibuya, I. A Neutron Diffraction Study of the Ferroelectric Transition of CsH_2PO_4. *J. Phys. Soc. Jpn.* **1980**, *49*, 304−307.
(53) Ichikawa, M. Hydrogen-bond Geometry and Its Isotope Effect in Crystals with OHO Bonds-Revisited. *J. Mol. Struct.* **2000**, *552*, 63−70.
(54) Xue, X.; Kanzaki, M. Proton Distributions and Hydrogen Bonding in Crystalline and Glassy Hydrous Silicates and Related Inorganic Materials: Insights from High-Resolution Solid-State Nuclear Magnetic Resonance Spectroscopy. *J. Am. Ceram. Soc.* **2009**, *92*, 2803−2830.
(55) Ichikawa, M. The O−H vs O···O Distance Correlation, the Geometric Isotope Effect in OHO Bonds, and Its Application to Symmetric Bonds. *Acta Crystallogr., Sect. B* **1978**, *34*, 2074−2080.
(56) Brown, I. On the Geometry of O−H···O Hydrogen Bonds. *Acta Crystallogr., Sect. A* **1976**, *32*, 24−31.
(57) Sternberg, U.; Brunner, E. The Influence of Short-Range Geometry on the Chemical Shift of Protons in Hydrogen Bonds. *J. Magn. Reson., Ser. A* **1994**, *108*, 142−150.
(58) Maricq, M. M.; Waugh, J. S. NMR in Rotating Solids. *J. Chem. Phys.* **1979**, *70*, 3300−3316.
(59) Thrippleton, M. J.; Cutajar, M.; Wimperis, S. Magic Angle Spinning (MAS) NMR Linewidths in the Presence of Solid-state Dynamics. *Chem. Phys. Lett.* **2008**, *452*, 233−238.
(60) Abragam, A. *The Principles of Nuclear Magnetism*; Clarendon Press: London, 1961.
(61) Steigel, A. *Dynamic NMR Spectroscopy*; Springer-Verlag: Berlin, 1978.
(62) Bloembergen, N.; Purcell, E. M.; Pound, R. V. Relaxation Effects in Nuclear Magnetic Resonance Absorption. *Phys. Rev.* **1948**, *73*, 679−712.
(63) Eckert, H.; Yesinowski, J. P.; Silver, L. A.; Stolper, E. M. Water in Silicate Glasses: Quantitation and Structural Studies by Proton Solid Echo and Magic Angle Spinning NMR Methods. *J. Phys. Chem.* **1988**, *92*, 2055−2064.
(64) Phillips, B. L.; Burnley, P. C.; Worminghaus, K.; Navrotsky, A. ^{29}Si and ^{1}H NMR Spectroscopy of High-pressure Hydrous Magnesium Silicates. *Phys. Chem. Miner.* **1997**, *24*, 179−190.
(65) Brinkmann, A.; Kentgens, A. P. M. Proton-Selective $^{17}O-^{1}H$ Distance Measurements in Fast Magic-Angle-Spinning Solid-State NMR Spectroscopy for the Determination of Hydrogen Bond Lengths. *J. Am. Chem. Soc.* **2006**, *128*, 14758−14759.
(66) MacKenzie, K. J. D.; Smith, M. E. *Multinuclear Solid-state NMR of Inorganic Materials*; Pergamon: New York, 2002.